A COMPREHENSIVE STUDY ON TROPICAL (10°N-15°N) MESOSPHERIC INVERSION LAYERS USING LIDAR AND SATELLITE (TIMED-SABER) OBSERVATIONS

K. Ramesh [1,*] , S. Sridharan [2], K. Raghunath [2]

[1] National Center for Atmospheric Research (NCAR), UCAR, Boulder, CO, USA.
[2] National Atmospheric Research Laboratory (NARL), Gadanki, A.P., India.

Email: [*] karanamram@gmail.com, susridharan@narl.gov.in, kraghunath@narl.gov.in

ABSTRACT

One of the interesting and poorly understood features of mesosphere and lower thermosphere (MLT) region is the phenomenon of Mesospheric Inversion Layers (MILs). The poor understanding of MILs is due to limited access of their occurrence height region, however the lidars are more efficient tools which provide stratosphere and mesosphere nocturnal temperatures with high temporal and vertical resolutions. The state-of-the-art lidar system comprising Mie, Rayleigh lidars installed at National Atmospheric Research Laboratory (NARL), Gadanki (13.5°N, 79.2°E), India has provided an excellent opportunity to undertake this study. The Nd:YAG laser source with lower power (11W) has been replaced by the one with higher power (30W) in January 2007. As the laser power has been increased, the molecular back scatter signal is also increased and consequently the top height level of the temperature retrieval has been increased to ~90-95 km. In the present study, the role of dominant causative mechanisms for the occurrence of MILs has been discussed using mainly the lidar and satellite (TIMED-SABER) observations over Gadanki region.

1. INTRODUCTION

Mesospheric Inversion Layer (MIL) is the region of temperature gradient inversion from negative to positive in mesosphere, over several kilometers in thickness [1,2,3]. The study of MILs is essential for the comprehensive understanding of middle atmosphere/MLT energy budget. Alhough the MILs have been reported from several sites using lidar and space borne observations, their morphological characteristics are still unknown. However their causative mechanisms are quite complex, the MILs occur mainly due to Gravity Wave (GW) breaking, Planetary Wave (PW) critical level interaction, chemical heating and GW-Tidal interaction [2,3]. In the absence of damping, all the atmospheric waves *viz*., GWs, PWs and Tides propagate vertically with exponentially ($e^{z/2H}$, z=altitude and H=scale height) increasing amplitudes in response to decreasing density up to MLT region. The waves deposit energy and momentum in the background when they break and consequently influence the thermal, dynamical structures and also the chemical composition. In addition to the above dynamical processes, the heating due to several exothermic reactions mainly among H, O, O_2, O_3, OH, HO_2 enhances the background temperature which is maintained as a MIL.

2. METHODOLOGY

2.1. The Gadanki Lidar System

The lidar system containing Mie, Rayleigh lidars installed at National Atmospheric Research laboratory (NARL), Department of Space, Gadanki (13.5°N, 79.2°E), India is operational since 1998. The system operates at 532 nm green laser with pulse repetition frequency (PRF) of 20 Hz and the relatively lower energy of ~550 mJ per pulse (PL8020, Continuum, USA). Later in 2007, the lidar system was upgraded with a high power laser of energy ~600 mJ/pulse and PRF of 50 Hz (PL9050, Continuum, USA) which is operated in monostatic biaxial mode. The 10X beam expander is used to expand the beam from its initial diameter of 9 mm to 90 mm so that the beam divergence decreases from ~0.45 mRad

to < 0.1 mRad and thus the beam remains within the field of view (FOV) of the receiving telescope at all height ranges. The Schmidt-Cassegrain (ø=35 cm) and Newtonian (ø=75 cm) telescopes serve as receivers to collect the atmospheric back scattered photons due to Mie (aerosols and clouds) and Rayleigh scattering (molecules) respectively. The received photons then allowed to fall on photo multiplier tubes (PMTs) of various gains (Hamamatsu, R3234-01). The PMT output signal will be collected and processed through the MCS-plus (Multi Channel Scalar) PC based photon count system with each two data acquisition channels of the receivers (Mie receiver:P, S channels & Rayleigh receiver : R, U channels). The photons are integrated for the time resolution of ~4 min corresponding to 12500 laser shots with dwell time of 2μsec for range resolution of 300 m. The laser source and the 90 mm expanded laser beam are shown in Figure 1(a-c).

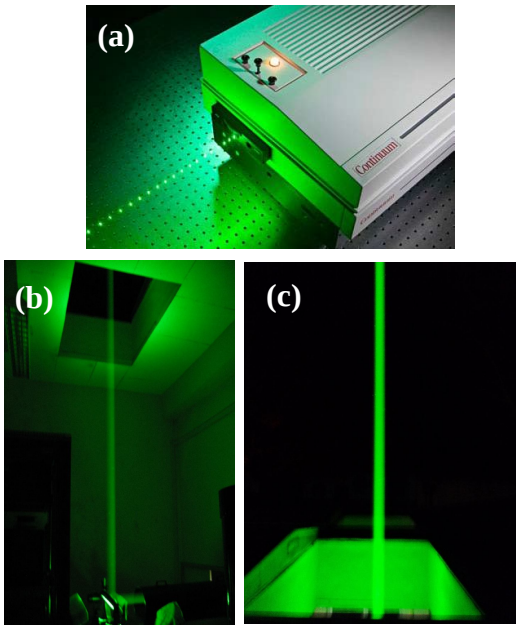

Figure 1. (a) Laser source from Continuum, USA (www.continuumlasers.com), (b) 90 mm beam steered upwards by a mirror, (c) beam entering into atmosphere.

The lidar equation for the backscattered photon counts can be given as follows.

$$N(z_i) = \frac{N_0 AKT^2(z_0, z_i)}{4\pi(z_i - z_0)^2}\left|n_r(z_i)\beta_r + n_m(z_i)\beta_m\right|\Delta z \quad \ldots\ldots\ldots (1)$$

where
z_i=Altitude of ith layer
N_i =Backscattered signal from i th altitude layer,
N_0=Number of emitted photons,
$n_r(z_i)$ & $n_m(z_i)$=Air molecules and aerosols concentrations,
β_r & β_m=Rayleigh and Mie backscattering cross sections,
z_0=Altitude of the lidar site,
A=Area of the receiver telescope,
$T^2(z_0,z_i)$=Atmospheric transmission,
K=Optical efficiency of the lidar system,
Δz=Thickness of the layer

The simulated lidar signal from equation (1) is as shown in Figure 2. The photon counts decreases with height in response to the decreasing atmospheric density.

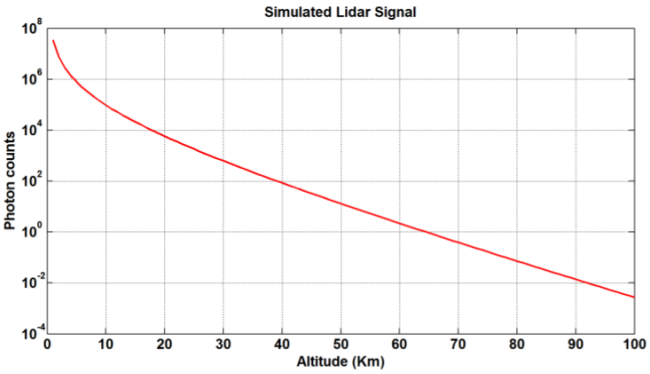

Figure 2. The simulated lidar signal for the lidar system at NARL, Gadanki.

2.2. Lidar Temperature Retrieval

The lidar temperature profiles are determined from the method given by *Hauchecorne and Chanin*,[1980] [4]. Above 30 km where the aerosol (Mie scattering) contribution is negligible and assuming the atmosphere is in hydrostatic equilibrium and obeys ideal gas law, the temperature at ith layer can be given by the following equation.

$$T(z_i) = \frac{M\,g(z_i)\Delta z}{R\,Log(1+X)} \quad \text{where } X = \frac{\rho(z_i)g(z_i)\Delta z}{P(z_i + \Delta z/2)} \quad \ldots\ldots\ldots\ldots (2)$$

and the statistical standard error in the temperature is given by the following equation.

$$\frac{\delta T(z_i)}{T(z_i)} = \frac{\delta Log|1+X|}{Log|1+X|} = \frac{\delta X}{(1+X)\,Log(1+X)} \qquad \text{.....(3)}$$

The scattering ratio is used to identify the aerosol and molecular layers and it can be defined as

$$R(z_i) = \frac{n_r(z_i)\beta_r + n_m(z_i)\beta_m}{n_r(z_i)\beta_r} \qquad \text{.....(4)}$$

In general, the scattering ratio is assumed to be unity above 30 km so that the contribution from aerosol scattering is negligible.

2.3. TIMED-SABER Observations

The Sounding of the Atmosphere using Broadband Emission Radiometry (SABER) is one of the four space-borne instruments onboard NASA's Thermosphere-Ionosphere-Mesosphere Energetics and Dynamics (TIMED) satellite. It provides vertical profiles of temperature, ozone volume mixing ratio (O_3 vmr), chemical heating rates due to various exothermic chemical reactions among H, O, O_2 , O_3 , OH, OH_2 , and volume emission rates of different species. More details on SABER instrument and different data sets can be obtained from *Remsberg et al*. [2003] [5], *Mlynczak et al*. [2007] [6], and *Gan et al*. [2012] [7].

3. OBSERVATIONS AND RESULTS

The nightly (19:07-23:14 LT) mean Rayleigh lidar temperature (T) over Gadanki along with TIMED-SABER temperature profile for 12.5°N, 79.0°E at 23:58 LT are shown in Figure 3a. The lidar and SABER temperature profiles show large inversion layers above ~75 km with amplitude and thickness of ~93 K, ~85 K and ~8 km, ~5 km respectively. The MSIS-90 (Mass Spectrometer Incoherent Scatter-90) model temperature profile also included in the figure for reference. The profiles of lapse rate, Γ=-dT/dz and the Brunt-vaisala frequency square (N^2) calculated from equation (5) are shown in Figure 3b and Figure 3c respectively. The lapse rate and N^2 values represents the presence of turbulent layers and conditions for convective instability.

$$N^2(z) = \frac{g(z)}{T(z)}\left[\frac{dT(z)}{dz} + \frac{g(z)}{c_p}\right] \qquad \text{.....(5)}$$

Here g(z), T(z) and c_p are acceleration due to gravity, mean temperature and specific heat at constant pressure (1004 J/K/Kg) respectively.

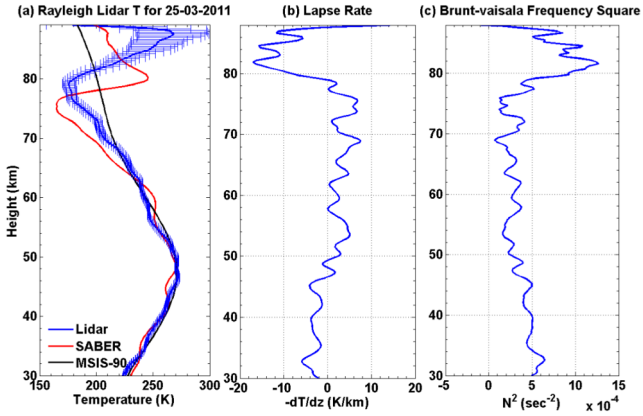

Figure 3. (a) lidar, TIMED-SABER and MSIS-90 temperatures, (b) lapse rate (-dT/dz), (c) Brunt-vaisala Frequency square (N^2) on the night of 25-03-2011 over Gadanki region.

It is evident from Figure 3b that the turbulent layers are not present as the lapse rate (Γ) is not equal to the adiabatic lapse rate (Γ_d ~10 K/km). Further it can be observed from Figure 3c that the condition for convective instability (N^2 <0) is not satisfied above ~75-80 km which indicates the negligible role of gravity wave breaking for the occurrence of inversion layer. Further the SABER chemical heating rates among H, O, O_2, O_3, OH and HO_2 for 25-03-2011 are shown in Figure 4. The reactions are listed in Table 1.

Table 1. Potential Exothermic Reactions for Mesospheric Heating Rates.

S.No.	Reaction
R_1	$O+OH \rightarrow H+O_2$
R_2	$H+O_2+M \rightarrow HO_2+M$
R_3	$H+O_3 \rightarrow OH+O_2$
R_4	$O+HO_2 \rightarrow OH+O_2$
R_5	$O+O+M \rightarrow O_2+M$
R_6	$O+O_2+M \rightarrow O_3+M$
R_7	$O+O_3 \rightarrow O_2+O_2$

The heating rates increase above ~77 km and the reaction between H and O_3 dominates all the reactions with ~10 K/day. Also the total heating rates are about 20 K/day in the inversion region at ~80 km.

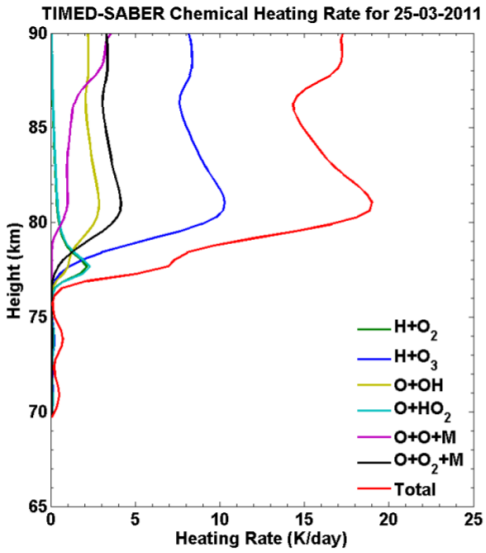

Figure 4. SABER chemical heating rates among H, O, O_2 , O_3 , OH, HO_2 for 25-03-2011.

4. SUMMARY AND DISCUSSION

The increased laser power of the NARL lidar system enabled to achieve the temperature profiles even up to ~90 km with the considerably lower uncertainty values. *Sridharan et al*. [2010] [8] observed a considerable reduction in the standard error with the new laser (PL9050) at heights ~5 km higher than the same obtained with the low power laser (PL8020). As an example, they obtained the standard error as 20 K at 85 km with low power laser and the same standard error is obtained above 90 km with the high power laser. They concluded that it is best suitable to study upper mesospheric temperature inversions, which takes place at altitudes above 85 km. In this study, it is clearly evident that the dynamics in connection with gravity wave breaking is negligible that can be observed primarily from the vertical profiles of lapse rate and Brunt-vaisala frequency square values. However the total chemical heating due to the exothermic reactionsamong H, O, O_2 , O_3, OH, HO_2 is dominant for the occurrence of the MIL with the total heating rate of ~20 K/day above ~75-80.

5. ACKNOWLEDGEMENTS

The authors thank the technical staff for operating and maintaining the Mie-Rayleigh lidar system at NARL, Gadanki, India. They also gratefully acknowledge the NASA's TIMED-SABER team for providing the data used in this study through the website: http://saber.gats-inc.com/. One of the authors, K. Ramesh acknowledges NCAR/UCAR for NASA's Jack-Eddy Postdoctoral Fellowship.

6. REFERENCES

[1] T. Leblanc and A. Hauchecorne, Recent observations of mesospheric temperature inversions, J. Geophys. Res., 102, 19471-19482 (1997).

[2] J. W. Meriwether, and A.J. Gerrard, Mesosphere inversion layers and stratosphere temperature enhancements, Rev. of Geophys., 42, RG3003 (2004).

[3] W. J. Meriwether, and C.S. Gardner, A review of the mesospheric inversion layer phenomenon, J. Geophys. Res., 105, 12405– 12416 (2000).

[4] A. Hauchecorne, and M.L. Chanin, Density and temperature profiles obtained by lidar between 35 and 70 km, Geophys. Res. Lett., 7, 565–568 (1980).

[5] E. Remsberg et al., On the verification of the quality of SABER temperature, geopotential height, and wind fields by comparison with Met Office assimilated analyses, J. Geophys.Res., 108(D19), 4628, doi:10.1029/2003JD003720 (2003).

[6] M.G. Mlynczak et al., Sounding of the Atmosphere using Broadband Emission Radiometry observations of daytime mesospheric $O_2(^1\Delta)$ 1.27 μm emission and derivation of ozone atomic oxygen, and solar and chemical energy deposition rates, J. Geophys. Res., 112, D15306, doi:10.1029/2006JD008355 (2007).

[7] Q. Gan et al, TIMED/SABER observations of Lower mesospheric inversion layers at low and middle latitudes, J. Geophys. Res., 117, D07109, doi:10.1029/2012JD017455 (2012).

[8] S. Sridharan et al., Near simultaneous lidar observations of upper mesospheric inversion layers and sporadic sodium layers over Gadanki (13.5°N, 79.2°E, Asian J. Phys., 19, 4, 13-18 (2010).